Haze and Thin Cloud Removal via Sphere Model Improved Dark Channel Prior

Jiayuan Li, Qingwu Hu, and Mingyao Ai

***Abstract*— Haze and cloud seriously degrade the quality of optical remote sensing images, which largely decrease their interpretability and intelligibility. In this letter, we propose a two-stage haze and thin cloud removal method based on homomorphic filtering (HF) and sphere model improved dark channel prior (DCP). Compared with current dehazing methods, the most advantage of the proposed method is that our method can deal with uneven haze, thick haze, and thin cloud. We observe that haze and cloud are highly related to the illumination component and mainly located in the low frequency of an image. Thus, we adapt HF to enhance the haze image, which makes the distribution of haze more even. In the second stage, we analyze the drawback of DCP, i.e., the transmission estimated by DCP is very sensitive to noise. To draw this issue, we propose a novel sphere model to estimate a more accurate transmission map. The sphere model improved DCP is more suitable for thick haze images than the traditional DCP. Extensive experimental results show that the proposed method significantly outperforms the compared state-of-the-art methods. The source code and data sets used in the letter are made public.[1]**

***Index Terms*— Dark channel prior (DCP), haze removal, homomorphic filtering (HF), sphere model, thin cloud removal, transmission.**

I. Introduction

DURING image acquisition stage, sensor imaging process is very sensitive to climatic factors and atmospheric conditions. Generally, the observed optical remote sensing images will be seriously degraded by the bad atmospheric conditions, which will largely decrease their interpretability and intelligibility. This phenomenon is called atmospheric attenuation. Atmospheric attenuation caused by haze and cloud not only affects the visual effect of observed images, but also brings challenges for subsequent image processing and analysis. Thus, haze and cloud removal is the basis of many visible image processing applications, which has very important practical value.

Haze and cloud removal is a very challenging issue. First, image patches covered by both haze and cloud contain the haze and cloud information and object feature information (radiation and texture). Haze and cloud removal may affect the object features. Second, haze and cloud are highly related to the elevations of objects. However, the elevation information of image scene is unavailable. If the degraded image is the only input, this issue becomes an under-constrained problem [1]. Therefore, many methods that use multiple images to increase constraints are proposed, such as methods based on multiple images of the same scene and methods based on depth maps. However, these methods are difficult to operate and their applicability is not strong. In many applications, such additional information is not unavailable. Recently, significant progress has been made in single-image haze.

In computer vision, image dehazing methods can be roughly grouped into four categories.

1) *Image Enhancement-Based Methods [2], [3]*: Tan [3] observed that haze-free images have higher contrast than haze images, so the radiance is restored by maximizing local contrast. These enhancement methods generally do not consider the atmospheric scattering model, which will get unsatisfactory performance under complex scenes.
2) *Prior- or Assumption-Based Methods*: He *et al.* [1] proposed a statistics prior called dark channel prior (DCP) for haze removal. Berman and Avidan [4] presented a nonlocal prior. This prior assumes that intensity values in a haze-free image can be approximated by some distinct intensity values.
3) *Fusion-Based Methods [5], [6]*: Ancuti and Ancuti [5] proposed a Laplacian pyramid multiscale fusion method, which blended two image inputs derived by contrast enhancement and white balance algorithms. Fusion methods do not suffer from patch-based artifacts and are very efficient. However, their performance are limited if the haze is dense or the images are dark.
4) *Deep Learning-Based Methods [7], [8]*: Cai *et al.* [8] developed an end-to-end dehazing system based on convolutional neural networks, called DehazeNet, for transmission map estimation. The results of these methods generally highly rely on the training data sets.

In remote sensing, traditional methods usually apply absolute atmospheric correction model to eliminate the atmospheric attenuation. However, the results highly rely on the accuracy of the atmospheric properties and sensor profile [9]. Recently, a number of single optical remote sensing image haze and thin cloud removal methods are proposed. Chavez [10] developed a dark-object subtraction technique for haze removal. Zhang *et al.* [11] presented a haze optimized transformation method for Landsat satellite images based on the red and blue bands. Moro and Halounova [12] proposed a generalized dark-object subtraction algorithm for high-resolution satellite data. Shen *et al.* [13] proposed a filtering method in frequency domain called adaptive homomorphic filter. Similar to the enhancement-based methods, these methods are also not based on the atmospheric scattering model. They may suffer from serious

Manuscript received May 14, 2018; revised August 15, 2018 and September 11, 2018; accepted September 28, 2018. Date of publication October 19, 2018; date of current version February 27, 2019. This work was supported by the National Natural Science Foundation of China under Grant 41701528. *(Corresponding author: Jiayuan Li.)*

The authors are with the School of Remote Sensing and Information Engineering, Wuhan University, Wuhan 430079, China (e-mail: ljy_whu_2012@whu.edu.cn; huqw@whu.edu.cn; aimingyao@whu.edu.cn).

Color versions of one or more of the figures in this letter are available online at http://ieeexplore.ieee.org.

Digital Object Identifier 10.1109/LGRS.2018.2874084

[1]http://www.escience.cn/people/lijiayuan/index.html

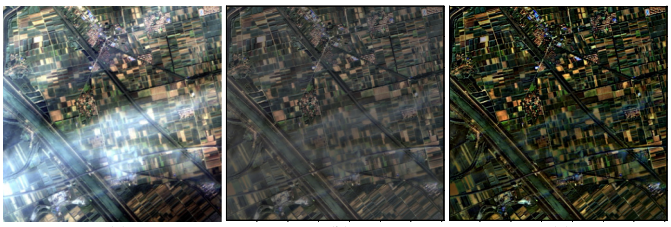

(a) (b) (c)

Fig. 1. Major stages in the proposed method. (a) Input image. (b) Result of haze distribution enhancement stage. (c) Final result via haze removal stage.

halo effects. Long *et al.* [14] improved the DCP by a low-pass Gaussian filter. Pan *et al.* [15] learned a data-driven deformed atmospheric scattering model based on the statistics of large amount of optical satellite images. The deformed DCP can effectively reduce color drifts. Liu *et al.* [16] proposed a ground radiance suppressed haze thickness map (GRS-HTM) for haze distribution estimation. However, the above techniques are not suitable for thick haze images.

In this letter, we develop a haze and thin cloud removal method based on homomorphic filtering (HF) and sphere model improved DCP. The proposed method is not only suitable for thin haze images, but also suitable for uneven and thick haze images. First, we use HF to improve the distribution of haze based on the observation that haze and cloud are highly related to illumination and located in the low frequency of an image. Second, we propose a novel sphere model to estimate a more accurate transmission map, which makes the proposed method more robust to thick haze. Both the qualitative and quantitative experimental results demonstrate the power of the proposed method.

II. Proposed Method

The proposed haze and thin cloud removal method consists of two major stages, i.e., haze distribution enhancement and haze removal. Fig. 1 shows its workflow. As illustrated, we first use HF to make the distribution of haze more even. Then, we use the proposed sphere model improved DCP to remove haze and thin cloud.

A. Haze Distribution Enhancement

Optical remote sensing images are often degraded by uneven haze and cloud, which are mainly caused by the atmospheric scattering. According to the atmospheric scattering model, the portion of the atmospheric radiation reaches the camera in a thick haze image region is more than the one in a thin image region. Thus, the illumination in the thick haze region is brighter than the one in the thin image region. In addition, haze and cloud have the same property with illumination; namely, they mainly locate in the low-frequency component of an observed image. We can enhance the uneven haze by making the illumination more even. Therefore, we apply HF to enhance the high-frequency component of the observed image and simultaneously suppress the low-frequency component.

HF is based on the illumination–reflectance model

$$\boldsymbol{I}(x) = \boldsymbol{J}(x)\boldsymbol{L}(x) \tag{1}$$

where x is an image pixel; $\boldsymbol{I}$ is the observed image; $\boldsymbol{J}$ is the true reflectance image; and $\boldsymbol{L}$ represents the illumination map. First, a logarithm operator is performed on both sides of the model, and the Fourier transformation is applied to convert the logarithm image into frequency domain

$$\Gamma\{\ln \boldsymbol{I}(x)\} = \Gamma\{\ln \boldsymbol{J}(x)\} + \Gamma\{\ln \boldsymbol{L}(x)\} = F_{\boldsymbol{J}} + F_{\boldsymbol{L}} \tag{2}$$

where $\Gamma\{\cdot\}$ represents the Fourier transformation; $\ln(\cdot)$ is a logarithm operator; and $F_{\boldsymbol{J}}$ and $F_{\boldsymbol{L}}$ are Fourier components. Then, a Gaussian high-pass filter $g(x)$ with standard deviation $\sigma_{g(x)}$ is performed to enhance the high frequency and suppress the low frequency, obtaining $F_{\hat{\boldsymbol{I}}}$

$$F_{\hat{\boldsymbol{I}}} = g(x)F_{\boldsymbol{J}} + g(x)F_{\boldsymbol{L}}. \tag{3}$$

Finally, the inverse Fourier transformation is applied to transform $F_{\hat{\boldsymbol{I}}}$ into space domain, and an exponential function is performed to get the illumination enhanced image $\hat{\boldsymbol{I}}$

$$\hat{\boldsymbol{I}} = \exp(\Gamma^{-1}\{F_{\hat{\boldsymbol{I}}}\}) \tag{4}$$

where $\Gamma^{-1}\{\cdot\}$ represents the Fourier transformation and $\exp(\cdot)$ is the exponential function.

B. Haze Removal

In the field of computer vision, the formation process of a haze or thin cloud image can be described by an atmospheric scattering model, whose mathematical expression is

$$\boldsymbol{I}(x) = \boldsymbol{J}(x)t(x) + \boldsymbol{A}(1 - t(x)) \tag{5}$$

where x is an image pixel; $\boldsymbol{I}$ is the hazy image digital values; $\boldsymbol{J}$ is the true image digital values; $\boldsymbol{A}$ represents the global atmosphere intensity vector; and $t(x)$ is the transmission of the atmosphere above the pixel x, which describes the portion of the electromagnetic radiation reaches the camera. The purpose of thin cloud or haze removal is to recover $\boldsymbol{J}$ from $\boldsymbol{I}$. Note that the proposed method regards the enhanced image $\hat{\boldsymbol{I}}$ as the observed image in (5).

1) Dark Channel Prior: DCP is *a priori* statistical law based on haze-free images, whose definition is: in most of nonsky region patches, there will be at least one spectrum band with very low intensity values on some pixels and tends to 0. The mathematical definition of DCP is as follows:

$$J_{\text{dark}}(x) = \min_{c\in\{r,g,b\}}\Big(\min_{y\in\Omega(x)}(J_c(y))\Big) \to 0 \tag{6}$$

where $\boldsymbol{J}_c$ is a spectrum band of $\boldsymbol{J}$, $c \in \{r, g, b\}$; $\Omega(x)$ is a small local image patch (an image patch represents a square local image region) with size S_Ω and centered at pixel x; and $\boldsymbol{J}_{\text{dark}}$ is the dark channel image.

There are three unknowns in (5), i.e., $\boldsymbol{A}$, t, and $\boldsymbol{J}$. To estimate the transmission t, DCP assumes that the atmosphere radiation vector $\boldsymbol{A}$ is estimated and the transmission in a local patch $\Omega(x)$ is constant, denoted by $\tilde{t}(x)$. First, (5) is divided by A_c on both sides, and then, the min operation is taken. According to (6), we have

$$\tilde{t}(x) = 1 - \min_{c\in\{r,g,b\}}\Big(\min_{y\in\Omega(x)}(I_c(y)/A_c)\Big). \tag{7}$$

In practice, to perceive depth, DCP introduces a constant parameter $w(0 < w < 1)$ into (7)

$$\tilde{t}(x) = 1 - w\min_{c\in\{r,g,b\}}\Big(\min_{y\in\Omega(x)}(I_c(y)/A_c)\Big). \tag{8}$$

Because the transmission $\tilde{t}(x)$ is constant in the local area $\Omega(x)$, it will inevitably cause block effects on the estimated

transmission map. Thus, DCP uses soft matting[2] [17] or guided filtering to obtain the optimized transmission map t. Once t is obtained, $\boldsymbol{J}$ can be recovered

$$\boldsymbol{J}(x) = \frac{\hat{\boldsymbol{I}}(x) - \boldsymbol{A}}{\max(t(x), t_0)} + \boldsymbol{A} \tag{9}$$

where t_0 is a parameter whose role is to avoid large noises.

2) Sphere Model Improved DCP: From (8), we know that the transmission $\tilde{t}(x)$ is decided by the minimal pixel intensity inside $\Omega(x)$. However, this will be seriously affected by noise. For example, if a local patch $\Omega(x)$ covered by haze and its pixel intensity is close to the atmosphere radiation, the true $\tilde{t}(x)$ of the local patch is close to 0. However, if there is a noise pixel in $\Omega(x)$ and its intensity is close to 0, the estimated $\tilde{t}(x)$ will be close to 1.

To deal with this issue, we have analyzed the distribution of pixels inside $\Omega(x)$ in the RGB color space and found that the pixel cluster region can be approximated by an ellipsoid. However, it is difficult to estimate an ellipsoid for each local patch. For efficiency, we use a sphere model instead. Let $\boldsymbol{i}_r^{\mathrm{T}} = (1, 0, 0)$, $\boldsymbol{i}_g^{\mathrm{T}} = (0, 1, 0)$, and $\boldsymbol{i}_b^{\mathrm{T}} = (0, 0, 1)$ be the unit length coordinate axes of the RGB color space, and $\boldsymbol{m} = [m_r, m_g, m_b] = [\hat{I}_r(y)/A_r, \hat{I}_g(y)/A_g, \hat{I}_b(y)/A_b]$ represents the normalized haze image pixel coordinates. Thus, (8) is equivalent to

$$\tilde{t}(x) = 1 - w \min_{c\in\{r,g,b\}} \big(\min_{y\in\Omega(x)} \big(i_c^{\mathrm{T}} m_c\big)\big). \tag{10}$$

According to the sphere distribution model, we have

$$f(\boldsymbol{m}) = (\boldsymbol{m} - \boldsymbol{u})^{\mathrm{T}}(\boldsymbol{m} - \boldsymbol{u}) \le R^2 \tag{11}$$

where $\boldsymbol{u}$ is the mean vector and R is the radius of the sphere. Generally, the radius R can be approximated by the standard deviation of pixels inside $\Omega(x)$. In the proposed method, we set $R = \sigma = (\sigma_r + \sigma_g + \sigma_b)/3$, where σ_c is the standard deviation of a channel of the local patch.

Suppose that vector $\boldsymbol{m}_c^*$ has the minimal $c \in \{r, g, b\}$ coordinate value among pixels inside $\Omega(x)$, $\boldsymbol{m}_c^*$ must be on the surface of the sphere and its unit normal vector is $-\boldsymbol{i}_c$. Thus, we have

$$f\big(\boldsymbol{m}_c^*\big) = \big(\boldsymbol{m}_c^* - \boldsymbol{u}\big)^{\mathrm{T}}\big(\boldsymbol{m}_c^* - \boldsymbol{u}\big) = \sigma^2 \tag{12}$$

$$\frac{\nabla_{\boldsymbol{m}} f\big(\boldsymbol{m}_c^*\big)}{\big\|\nabla_{\boldsymbol{m}} f\big(\boldsymbol{m}_c^*\big)\big\|} = -\boldsymbol{i}_c \tag{13}$$

where

$$\begin{aligned}\nabla_{\boldsymbol{m}} f\big(\boldsymbol{m}_c^*\big) &= \frac{\partial f(\boldsymbol{m})}{\partial \boldsymbol{m}}|_{\boldsymbol{m}=\boldsymbol{m}_c^*} \\ &= \frac{\partial(\boldsymbol{m}^T\boldsymbol{m} - 2\boldsymbol{m}^{\mathrm{T}}\boldsymbol{u} + \boldsymbol{u}^{\mathrm{T}}\boldsymbol{u})}{\partial \boldsymbol{m}}|_{\boldsymbol{m}=\boldsymbol{m}_c^*} \\ &= 2\big(\boldsymbol{m}_c^* - \boldsymbol{u}\big)\end{aligned} \tag{14}$$

Substituting (14) into (13), obtaining

$$\boldsymbol{m}_c^* - \boldsymbol{u} = -\boldsymbol{i}_c\big\|\boldsymbol{m}_c^* - \boldsymbol{u}\big\|. \tag{15}$$

Thus, (12) is equivalent to

$$\begin{aligned} f\big(\boldsymbol{m}_c^*\big) &= \big(-\boldsymbol{i}_c\big\|\boldsymbol{m}_c^* - \boldsymbol{u}\big\|\big)^{\mathrm{T}}\big(-\boldsymbol{i}_c\big\|\boldsymbol{m}_c^* - \boldsymbol{u}\big\|\big) \\ &= \big(\big\|\boldsymbol{m}_c^* - \boldsymbol{u}\big\|\big)^2 = \sigma^2 \\ &\rightarrow \big\|\boldsymbol{m}_c^* - \boldsymbol{u}\big\| = \sigma. \end{aligned} \tag{16}$$

[2]"soft matting" is an image processing technique in computer vision, which is used in the dark channel prior algorithm to refine the transmission map.

TABLE I
DATA SET INFORMATION

Satellite sensor	Number of images	GSD /m	Image size/pixels	Color mode	location
SkySat-1	10	0.8	1500×1500	False	California, USA
Landsat 8	10	30	1500×1500	True	Unknown
Gaofen-2	15	1	1000×1000	True	Jilin, China
IKONOS	5	1	580×380	True	Texas, USA
Gaofen-1	8	2	1920×965	True	Wuhan, China

TABLE II
PARAMETER $\sigma_{g(x)}$ STUDY

metric	$\sigma_{g(x)}$, $S_\Omega = 15\times15$, $w = 0.95$			
	5	10	15	20
IL-NIQE	29.72	**28.52**	29.23	30.56
BRISQUE	25.95	**25.42**	25.88	27.04

TABLE III
PARAMETER S_Ω STUDY

metric	S_Ω , $\sigma_{g(x)} = 10$, $w = 0.95$			
	5	15	25	45
IL-NIQE	31.66	**28.52**	28.84	29.61
BRISQUE	27.99	**25.42**	25.69	26.11

Equation (10) can be represented as

$$\begin{aligned}\tilde{t}(x) &= 1 - w \min_{c\in\{r,g,b\}} \big(\boldsymbol{i}_c^{\mathrm{T}}\boldsymbol{m}_c^*\big) \\ &= 1 - w \min_{c\in\{r,g,b\}} \big(\boldsymbol{i}_c^{\mathrm{T}}\big(\boldsymbol{u} - \boldsymbol{i}_c\big\|\boldsymbol{m}_c^* - \boldsymbol{u}\big\|\big)\big) \\ &= 1 - w \min_{c\in\{r,g,b\}} (u_c - \sigma)).\end{aligned} \tag{17}$$

After obtaining the transmission map, the dehazing step is the same as the DCP algorithm. Finally, we use a color transfer algorithm to remove color drifts.

III. EXPERIMENTAL RESULTS

The proposed method is compared with three other state-of-the-art methods, i.e., DCP method [1], nonlocal dehazing method [4], and GRS-HTM [16]. The experiments are performed on a laptop with i5, 2.5-GHz Intel Core CPU.

A. Data Set

We collect 48 satellite images for performance evaluation. These images are captured under the bad atmospheric conditions, such as haze, cloud, smoke, and fog. More details can be found in Table I. We choose Mean Absolute Error (MAE), Integrated Local Natural Image Quality Evaluator (IL-NIQE) [18], and the Blind/Referenceless Image Spatial QUality Evaluator (BRISQUE) [19] as evaluation metrics, where MAE measures the degree of color drift, and IL-NIQE and BRISQUE reflect the quality of an image without relying on ground truth reference images. We use eight Gaofen-1 images for MAE evaluation since these images contain both hazy regions and clear regions, and use other 40 images for IL-NIQE and BRISQUE evaluations.

B. Parameter Analysis

There are four main parameters in our method, i.e., the standard deviation $\sigma_{g(x)}$, the local patch size S_Ω, the constant parameter w, and the noise suppression parameter t_0. The role of t_0 is to prevent the divisor from being too small. Similar to other DCP-based methods, we set $t_0 = 0.1$. We carry out three

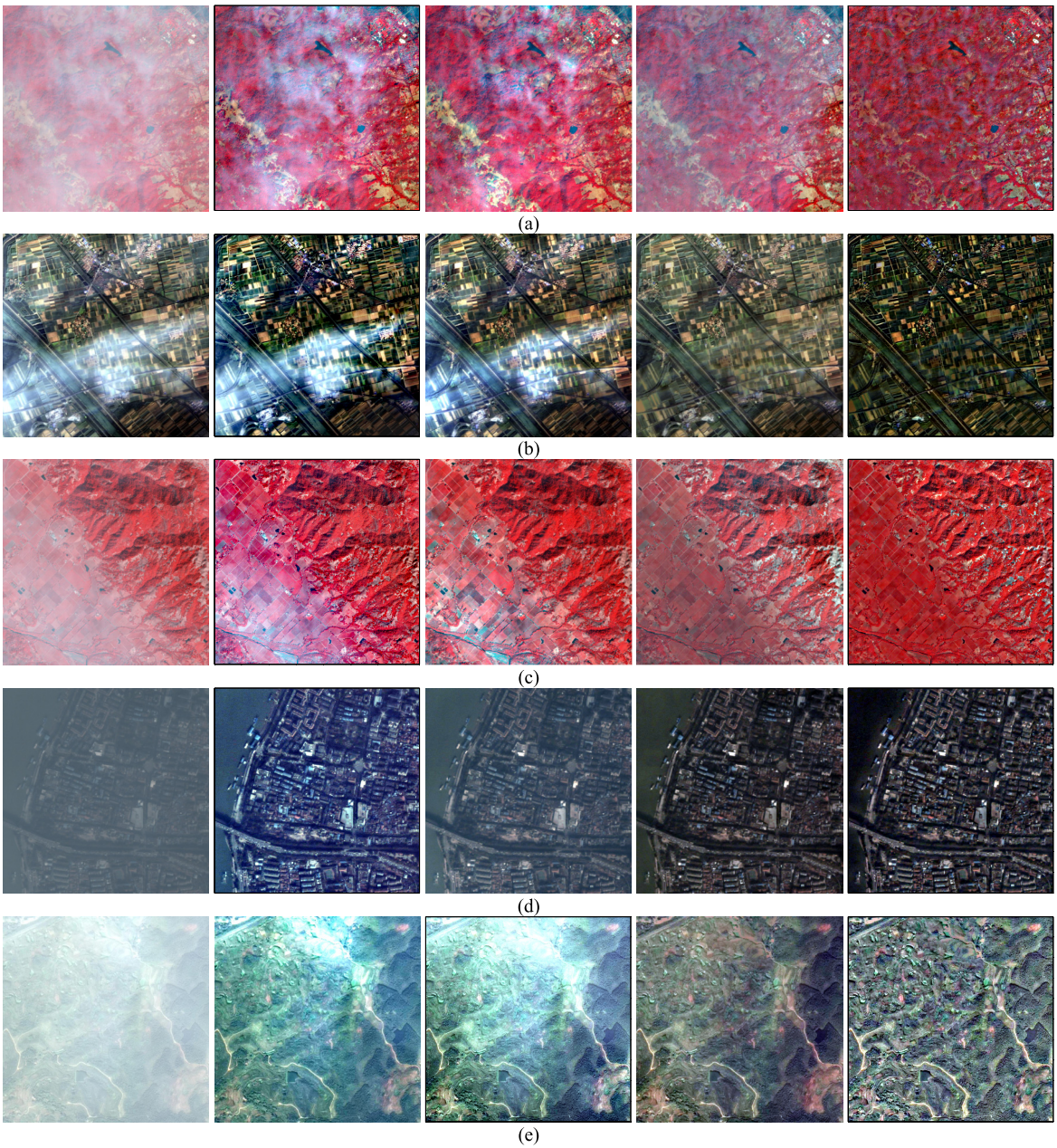

Fig. 2. Qualitative comparisons. (First column to fifth column) Selected input images, the results of nonlocal dehazing, the results of DCP, the results of GRS-HTM, and the results of the proposed method, respectively. (a) Results on the uneven smoke image. (b) Results on the uneven thin cloud image. (c) Results on the uneven haze image. (d) Results on the heavy smog image. (e) Results on the heavy fog image.

TABLE IV
PARAMETER w STUDY

metric	w, $S_\Omega = 15\times15$, $\sigma_{g(x)} = 10$			
	0.35	0.55	0.75	0.95
IL-NIQE	36.72	34.93	30.18	**28.52**
BRISQUE	32.16	30.17	26.33	**25.42**

experiments to study the parameters $\sigma_{g(x)}$, S_Ω, and w, where each experiment has only one parameter as variable, and others are constant. The results are reported in Tables II–IV.

From Tables II–IV, we can learn the following.

1) For parameters $\sigma_{g(x)}$ and S_Ω, both large and small values of them result in bad performance. The best result is achieved when $\sigma_{g(x)} = 10$ and $S_\Omega = 15 \times 15$.
2) Larger w results in better performance. Thus, we set $\sigma_{g(x)}$ to 10, S_Ω to 15×15 pixels, and $w = 0.95$.

All parameters are fixed throughout the experiment.

C. Qualitative and Quantitative Comparisons

Five typical images are selected for qualitative comparisons. In detail, the first image is a false color image captured in mountain areas, which is degraded by uneven smoke. The second image is captured over a farm, which suffers from uneven thin cloud. The ranges of elevations in the third image are very large, which results in uneven haze. The fourth and the last ones are degraded by heavy smog and fog, respectively.

The qualitative results are shown in Fig. 2(a)–(e), respectively. As can be seen, on the smoke image [Fig. 2(a)], nonlocal dehazing, DCP, and GRS-HTM can improve the over-

TABLE V
MAE COMPARISONS

MAE	Non-local dehazing	DCP	GRS-HTM	Ours
Red band/pixels	36.16	25.39	12.52	**9.56**
Green band/pixels	38.33	23.36	11.03	**7.26**
Blue band/pixels	42.62	23.88	13.29	**7.73**

TABLE VI
IL-NIQE AND BRISQUE COMPARISONS

metric	Observed images	Non-local dehazing	DCP	GRS-HTM	Ours
IL-NIQE	37.78	34.89	35.22	29.37	**28.52**
BRISQUE	34.96	28.95	29.36	26.87	**25.42**

TABLE VII
RUNNING TIME ANALYSIS

Image size/pixels	250× 250	500× 500	1000× 1000	1500× 1500	2000× 2000
HF time/s	0.25	0.54	1.38	4.51	7.89
Dehazing time/s	0.05	0.23	1.13	2.32	4.47
Total time/s	0.3	0.77	2.51	6.83	12.36

all quality. However, the corrected images of these methods still contain lots of heavy smoke. In contrast, our method performs much better. The result only contains a little thin smoke. Our dehazed image may look dim. This is expected, because pixels with influence of atmosphere have always higher digital values. On the uneven haze and cloud images [Fig. 2(b) and (c)], it is hardly to say that nonlocal dehazing and DCP improve the image quality. The distributions of haze (cloud) in the results of nonlocal dehazing and DCP become more uneven. The GRS-HTM performs well on Fig. 2(b) while bad in Fig. 2(c). On the contrary, the proposed method is very suitable for uneven haze problem. Our method can make the distribution of haze more even. Thus, our results are clearer and more natural. There is almost no haze (cloud) in the corrected images. On the thick smog image [Fig. 2(d)], nonlocal dehazing, GRS-HTM, and our method get very clear results, while DCP performs less satisfactory. The result of nonlocal dehazing suffers from serious color drift. On the thick fog image [Fig. 2(e)], both the results of nonlocal dehazing and DCP are overexposed and suffer from color drifts. The result of GRS-HTM is clear; however, it is less impressed than our result. In summary, our method achieves more balanced and sufficient dehazing results than other compared methods.

Table V reports the MAE comparisons. As shown, the color drift of the proposed method is the smallest. The GRS-HTM is much better than other two methods. Table VI reports IL-NIQE and BRISQUE comparisons. Again, the proposed method is the best in both metrics. The GRS-HTM ranks the second; nonlocal dehazing ranks the third; and DCP performs the worst.

Table VII analyzes the time efficiency of our method on an image sequence with different image sizes. As reported, the dehazing stage is fast, whose running time increases linearly with the image size. The HF stage is relatively slow. The total running time of our method on an image with 1500×1500 pixels is 6.8 s. However, as reported in [16], the GRS-HTM needs more than 20 s to perform an image with 1600×1600 pixels. Note that the running time of GRS-HTM is calculated on a hardware device with much better calculation performance. In addition, if the source code of our method is rewritten by C/C++, the time efficiency will be largely improved.

IV. CONCLUSION

This letter developed an effective technique for haze and thin cloud removal. We first used HF to improve the distribution of haze. Then, we proposed a sphere model improved DCP to process haze images. Compared with current dehazing methods, the advantage of the proposed method is that our method can deal with uneven and thick haze. Both the qualitative and quantitative experimental results show that the proposed method significantly outperforms the compared state-of-the-art methods, including the well-known DCP method, nonlocal dehazing method, and GRS-HTM method.

REFERENCES

[1] K. He, J. Sun, and X. Tang, "Single image haze removal using dark channel prior," *IEEE Trans. Pattern Anal. Mach. Intell.*, vol. 33, no. 12, pp. 2341–2353, Dec. 2011.
[2] J.-H. Kim, W.-D. Jang, J.-Y. Sim, and C.-S. Kim, "Optimized contrast enhancement for real-time image and video dehazing," *J. Vis. Commun. Image Represent.*, vol. 24, no. 3, pp. 410–425, Apr. 2013.
[3] R. T. Tan, "Visibility in bad weather from a single image," in *Proc. IEEE Conf. Comput. Vis. Pattern Recognit. (CVPR)*, Jun. 2008, pp. 1–8.
[4] D. Berman T. Treibitz, and S. Avidan, "Non-local image dehazing," in *Proc. IEEE Conf. Comput. Vis. Pattern Recognit.*, Jun. 2016, pp. 1674–1682.
[5] C. O. Ancuti and C. Ancuti, "Single image dehazing by multi-scale fusion," *IEEE Trans. Image Process.*, vol. 22, no. 8, pp. 3271–3282, Aug. 2013.
[6] A. Galdran, J. Vazquez-Corral, D. Pardo, and M. Bertalmío, "Fusion-based variational image dehazing," *IEEE Signal Process. Lett.*, vol. 24, no. 2, pp. 151–155, Feb. 2017.
[7] B. Li, X. Peng, Z. Wang, J. Xu, and D. Feng, "Aod-Net: All-in-one dehazing network," in *Proc. IEEE Int. Conf. Comput. Vis.*, Oct. 2017, pp. 4780–4788.
[8] B. Cai, X. Xu, K. Jia, C. Qing, and D. Tao, "DehazeNet: An end-to-end system for single image haze removal," *IEEE Trans. Image Process.*, vol. 25, no. 11, pp. 5187–5198, Nov. 2016.
[9] S. Liang, H. Fang, and M. Chen, "Atmospheric correction of Landsat ETM+ land surface imagery. I. Methods," *IEEE Trans. Geosci. Remote Sens.*, vol. 39, no. 11, pp. 2490–2498, Nov. 2001.
[10] P. S. Chavez, Jr., "An improved dark-object subtraction technique for atmospheric scattering correction of multispectral data," *Remote Sens. Environ.*, vol. 24, no. 3, pp. 459–479, Apr. 1988.
[11] Y. Zhang, B. Guindon, and J. Cihlar, "An image transform to characterize and compensate for spatial variations in thin cloud contamination of Landsat images," *Remote Sens. Environ.*, vol. 82, nos. 2–3, pp. 173–187, 2002.
[12] G. D. Moro and L. Halounova, "Haze removal for high-resolution satellite data: A case study," *Int. J. Remote Sens.*, vol. 28, no. 10, pp. 2187–2205, 2007.
[13] H. Shen, H. Li, Y. Qian, L. Zhang, and Q. Yuan, "An effective thin cloud removal procedure for visible remote sensing images," *ISPRS J. Photogramm. Remote Sens.*, vol. 96, pp. 224–235, Oct. 2014.
[14] J. Long, Z. Shi, W. Tang, and C. Zhang, "Single remote sensing image dehazing," *IEEE Geosci. Remote Sens. Lett.*, vol. 11, no. 1, pp. 59–63, Jan. 2014.
[15] X. Pan, F. Xie, Z. Jiang, and J. Yin, "Haze removal for a single remote sensing image based on deformed haze imaging model," *IEEE Signal Process. Lett.*, vol. 22, no. 10, pp. 1806–1810, Oct. 2015.
[16] Q. Liu, X. Gao, L. He, and W. Lu, "Haze removal for a single visible remote sensing image," *Signal Process.*, vol. 137, pp. 33–43, Aug. 2017.
[17] A. Levin, D. Lischinski, and Y. Weiss, "A closed-form solution to natural image matting," in *Proc. IEEE Comput. Soc. Conf. Comput. Vis. Pattern Recognit.*, vol. 1, Jun. 2006, pp. 61–68.
[18] L. Zhang, L. Zhang, and A. C. Bovik, "A feature-enriched completely blind image quality evaluator," *IEEE Trans. Image Process.*, vol. 24, no. 8, pp. 2579–2591, Aug. 2015.
[19] A. Mittal, A. K. Moorthy, and A. C. Bovik, "No-reference image quality assessment in the spatial domain," *IEEE Trans. Image Process.*, vol. 21, no. 12, pp. 4695–4708, Dec. 2012.